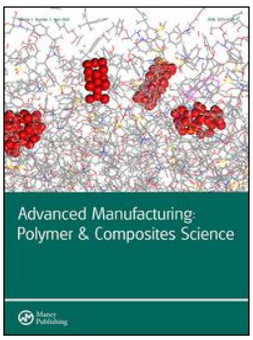

Taylor & Francis
Taylor & Francis Group

Advanced Manufacturing: Polymer & Composites Science

ISSN: 2055-0340 (Print) 2055-0359 (Online) Journal homepage: http://www.tandfonline.com/loi/yadm20

Molecular dynamics study on effects of aspect ratio of carbon nanotubes in thermosetting epoxy based nanocomposites including modeling of crosslinking process

Jung-Hoon Sul*, B. Gangadhara Prusty & Donald W. Kelly

To cite this article: Jung-Hoon Sul*, B. Gangadhara Prusty & Donald W. Kelly (2015) Molecular dynamics study on effects of aspect ratio of carbon nanotubes in thermosetting epoxy based nanocomposites including modeling of crosslinking process, Advanced Manufacturing: Polymer & Composites Science, 1:2, 94-104, DOI: 10.1179/2055035914Y.0000000009

To link to this article: http://dx.doi.org/10.1179/2055035914Y.0000000009

Published online: 09 Jan 2015.

AMPCS Advanced Manufacturing: Polymer & Composites Science

Original Research Paper

Molecular dynamics study on effects of aspect ratio of carbon nanotubes in thermosetting epoxy based nanocomposites including modeling of crosslinking process

Jung-Hoon Sul*, B. Gangadhara Prusty and Donald W. Kelly

School of Mechanical and Manufacturing Engineering, UNSW Australia, Sydney, NSW 2052, Australia

Abstract A comprehensive modeling and simulation approach using molecular dynamics (MD) is presented in this paper. The influence of aspect ratio of carbon nanotubes (CNTs) in thermosetting epoxy is studied using MD. The thermo-mechanical properties of epoxy models reinforced by CNTs with various aspect ratios are extracted. CNTs with the higher aspect ratio increase stiffness of the epoxy resin with facilitating premature yield in tension while a noticeable degradation in thermal properties is evidenced. The evolution of internal energy during straining shows that CNTs prolong the constant transition rate of dihedral and van der Waals energy in the elastic region. This might delay conformational changes of epoxy molecules to the lower energy level. Free volume and pair distribution function studies of the molecular models with CNTs compared with the neat epoxy model provide the plausible conclusion that the steric hindrance of CNTs in the three-dimensional epoxy molecular domain may result in the less dense structure of the epoxy.

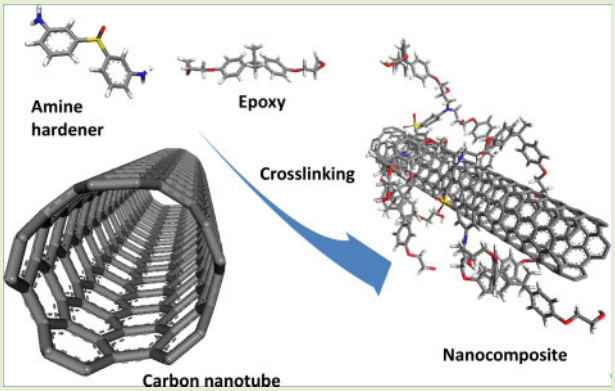

Keywords Carbon nanotubes, Thermosetting epoxy, Crosslinking, Thermo-mechanical characterization

Cite this article J.-H. Sul, B. Gangadhara Prusty and D. W. Kelly. *Adv. Manuf.: Polym. Compos. Sci.*, 2015, 1, 94-104

Introduction

Carbon nanotubes (CNTs) have attracted a considerable amount of attention from research communities in a wide variety of fields owing to their extraordinary electrical, thermal and mechanical properties.[1] Despite their exceptional potential for improving properties of current materials, their practical application has been stagnant due to issues with dispersion during manufacture. These issues can be even more serious in structural applications in which viscous polymeric resin is widely used as a matrix. There has been a substantial amount of research to disperse CNTs in polymeric resins such as thermosetting epoxy using various methods such as a chemical modification by means of functionalization[2,3] and physical mixing[1,4,5] including ultrasonication, extrusion, calendaring, etc. Although there is a wide range of dispersal methods that have been developed to deliver a relatively good dispersion state of CNTs in viscous polymer resins, the resulting states are not at the perfect stage. Furthermore, functionalization of CNTs can result in defects, catalytic effects of CNTs and the uncontrollable stoichiometry of the epoxy. In addition to the dispersion issues, the current mass-production processes of CNTs leave some challenges in the application of CNTs.[6] For example, the purity of CNTs and lack of tailoring their structure will affect performance of materials for engineering structures. Efficiency of CNTs in reinforcing polymer strongly depends on the crystalline structure of CNTs at atomic scale while load transferring from matrix to CNT through the intermediate phase between CNTs and surrounding polymer plays a key role at micro-scale.[7] However, resolving such issues is a matter of time as processing and characterization technologies are being advanced rapidly. On the fabrication side, for example, investigators[8,9] developed a new synthetic approach that can afford a flawless CNT with control of its structure and length.

*Corresponding author, email: j.sul@unsw.edu.au

Received 27 October 2014; accepted 16 December 2014
DOI 10.1179/2055035914Y.0000000009

Maney Publishing

Computer simulation, in the meantime, has provided a successful and attractive complement to empirical or experimental research in numerous fields in which real-life technologies are too costly or yet to be successfully implemented. Simulations at the atomic level have been successfully applied in the pharmaceutical industry and have potential to guide the research effort by simulating the properties of novel materials.[10] Among those atomistic simulation methods, molecular dynamics (MD) has been acknowledged to be a powerful method for providing a better understanding of the role of atomistic structures of materials at the macroscopic scale.[11] However, studies using MD for cross-linked epoxy in literature are limited with minimal consideration of the physical chemistry compared to other materials because the molecular structures of epoxy promotes highly strained local regions with high local crosslink density.[12] There have been a limited number of studies[10,13–16] involving cross-linked epoxy models that are chemically and physically valid with a development of molecular modelling techniques and improved computing performance. These studies focus mainly on extracting thermo-mechanical properties of existing material systems and show good agreement with experimental data. The materials science and mechanical engineering community has now directed their focus to the development of new material systems using MD. Published work on the theoretical[17] and experimental[18] investigations report that aspect ratio of CNTs is an important parameter affecting the amount of stress transfer from a matrix to CNTs in composite materials to a great extent. Zho *et al.*[19] also investigated the effects of CNT length on strain-stress behavior of epoxy resin using two different CNT lengths and demonstrated that longer CNTs increased the Young's modulus of the epoxy resin by 10 times whereas shorter CNTs provided 20 % higher Young's modulus than the neat epoxy. Coto *et al.*[20] studied the influence of the geometrical properties of CNTs on the interaction with epoxy by a pull-out simulation. They claimed that the length of a CNT played a significant role in determining the interfacial strength between CNTs and epoxy rather than the diameter or chirality of the CNT. While the influences of CNT aspect ratio on stiffness and strength of nano-composites have been fruitful, its effect on thermal properties and curing behavior of the epoxy resin has not been deeply explored.

In this paper, the atomistic modeling and MD simulation methodology is described in detail. The main objective of this research is to model the realistic structure of diglycidyl ether of bisphenol-A (DGEBA) cured with 3,3'-diamino diphenyl sulfone (3,3'-DDS) that is widely used in the aerospace engineering and to quantitatively investigate the effect of CNT additives with various aspect ratios on the thermo-mechanical performance of the epoxy resin. The atomistic modeling methodology presented in this study is a dendrimer building approach derived from repetitively branched molecules. Highly branched molecules radiating from a central seed monomer via a stepwise procedure can ensure physical and chemical validity of the model. Simulation algorithms are developed to evaluate the thermal properties in an isobaric simulation process and the mechanical properties under uniaxial deformation. In addition, the importance of epoxy molecular weight has been neglected in MD simulations while it has been a significant topic of experimental studies[21–23] for decades. This study attempts to overcome limitations of the previous modeling works that cannot control the epoxy equivalent weight of the atomistic model. The results based on four different models with various aspect ratios of CNTs are compared and discussed. The simulation results with the different reinforcement are further investigated by considering other properties, including the free volume of the molecular structures modeled, pair distribution functions of crosslinks and decomposition of the potential energy evolution.

Molecular modeling and simulation methods

The methodology used to generate the atomistic models and crosslinks, and calculate thermo-mechanical properties using MD is elaborated in this section.

Modeling constituents of epoxy and its cross-linking

The epoxy system chosen in this study is DGEBA, commercially known as EPON 825, cross-linked with 3,3'-DDS whose chemical structures are depicted in Fig. 1. All of the constituent monomer, oligomer and reinforcements were modelled in a commercial MD simulation package, Materials Studio 6.0.[24] The charge equilibration (QEq) approach[25] was used to predict the partial charge distribution to each atom composing the molecules as depicted in Fig. 2*a*. Based on the charge calculation, atoms that make a neutral charge summation in the monomers were grouped together. The size of each group is within the range of 3 Å determined from the van der Waals radii of the atoms for using the group summation of electrostatic and van der Waals energy. The group summation enables not only rapid non-bond energy calculations, but also allows prevention of fluctuations near a cut-off distance that can occur if pairwise only interactions of atom based summation are used. Furthermore, the neutrally charged group ensures the dipole-dipole interaction in the electrostatic interaction between a pair of groups so that erroneous monopole terms are not introduced.[26]

The crosslinking process adopted in this study followed the dendrimer modelling approach on the literature,[11,12,27] constructing a highly branched polymer structure. Chemical reactions were not simulated in this study so that each of the

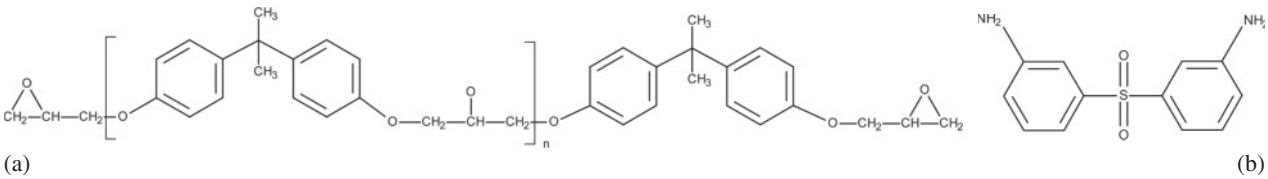

Figure 1 Chemical structures of *a* diglycidyl ether of bisphenol-A and *b* meta-substituted 3,3'-diamino diphenyl sulfone

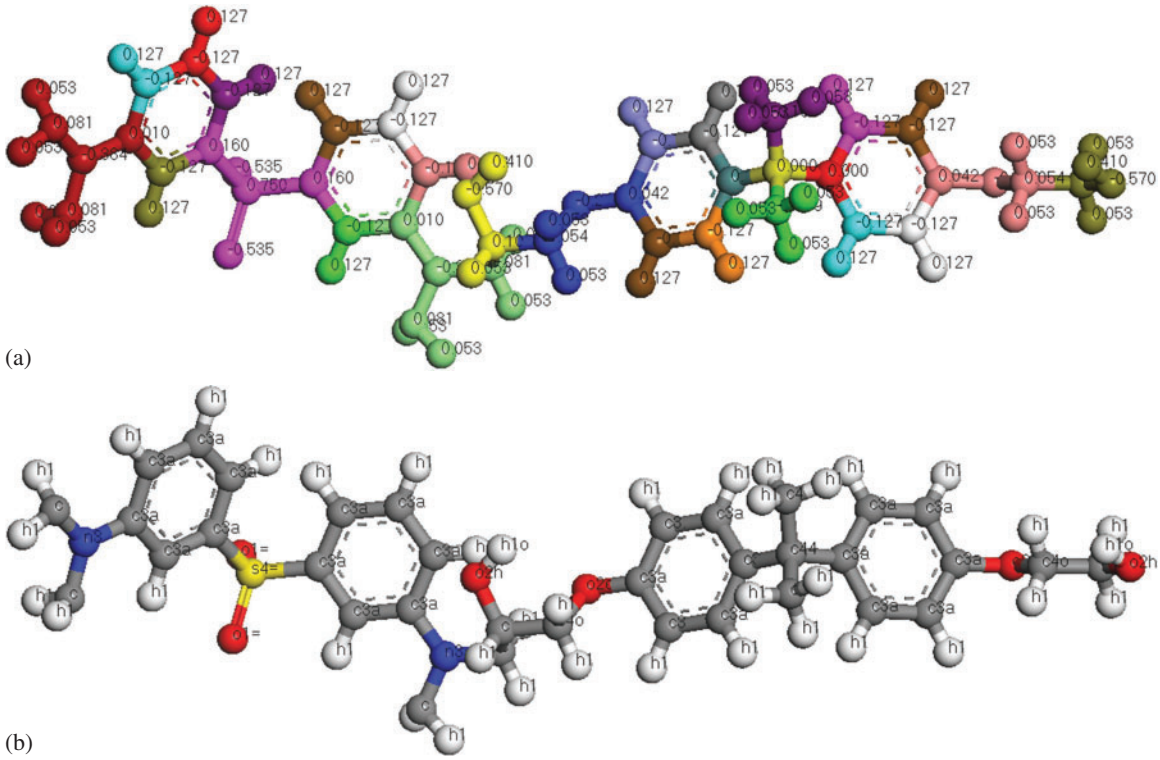

Figure 2 Polymerised set of DGEBA and 3,3'-DDS showing *a* charge in coulomb of each atom for group summation of electrostatic and van der Waals energy and *b* force field type for each atom

oligomer and monomers required to be modified to replicate the cross-linked structure. The polymerization procedure is illustrated in Fig. 3 showing the following steps:

(1) the highly strained oxirane ring in DGEBA and the reactive amine group in 3,3'-DDS;
(2) the epoxide ring is opened by moving the alpha carbon atom to the amine group in 3,3'-DDS. A hydrogen atom is added to the epoxide oxygen atom to form an alcohol group. One of the hydrogen atoms attached to the beta carbon atom in DGEBA is designated as a connecting site shown in the red cages;
(3) each of the connecting hydrogens is removed so that the alpha and beta carbon atoms are connected again to create the covalent bond between the epoxide and amine groups. This allows maintaining the continuous neutral charge group even after the polymerization procedure.

The base epoxy, DGEBA, that consists of a repetitive pair of bisphenol-A and epichlorohydrin has 0.05 of the average number of bisphenol-A moiety based on the experimental molecular weight. To match the molecular weight of the epoxy model with the experimental value, molecular models with two different degrees of polymerization were prepared, one with $n = 2$ and another with $n = 0$. A seven generation dendrimer was built in stoichiometric proportion as illustrated in Fig. 4 using the polymerization scheme outlined above. In the dendrimer modelling process, the DGEBA oligomer model with

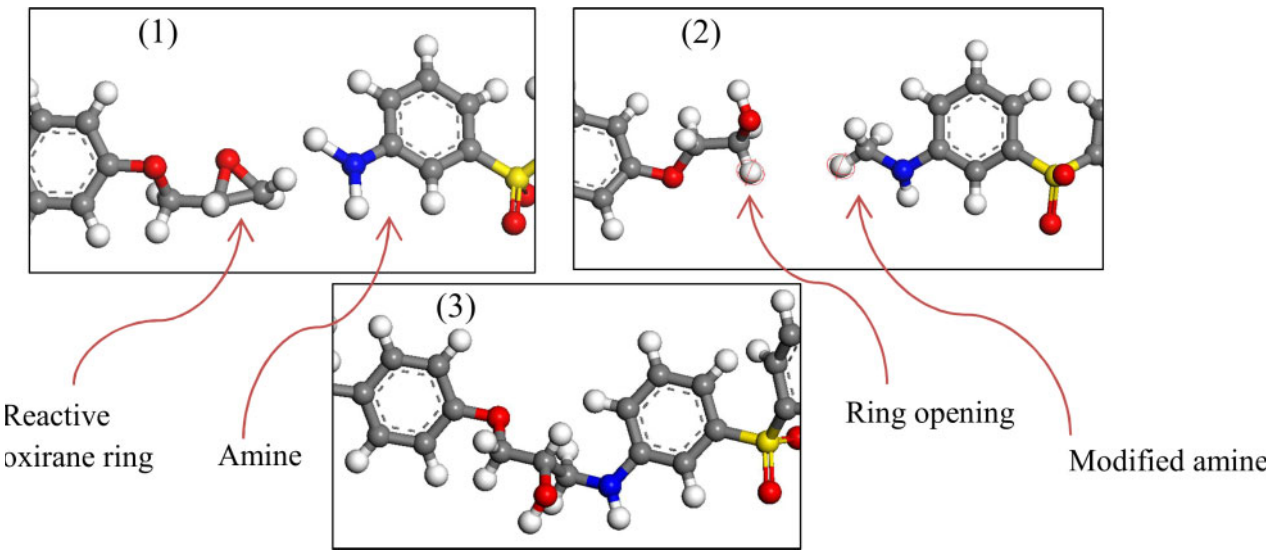

Figure 3 Schematic illustration of polymerisation process

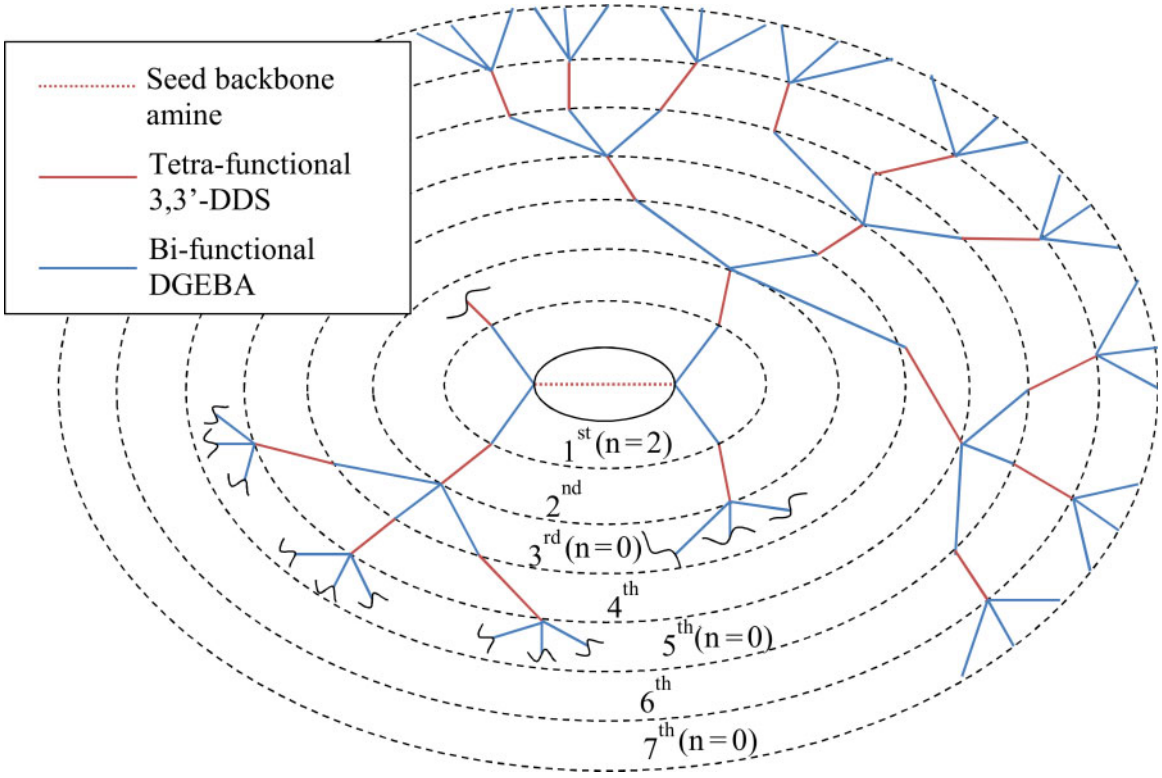

Figure 4 Schematic representation of dendrimer model used in this study

$n = 2$ was used in the first generation of the dendrimeric model while the rest of generations for DGEBA (i.e. third, fifth and seventh generations) consisted of the model with $n = 0$. The resultant molecular weight in Table 1 shows very good agreement with the experimental data obtained from the manufacturer of the commercial DGEBA.

Atomistic modeling of carbon reinforcements

Three different carbon structures were modeled and used as reinforcement in the epoxy resin modeled previously. All carbon structures modeled in this study were the armchair single walled CNTs with the chiral indices of (5,5), which makes the diameter of all reinforcements 6.78 Å. As illustrated in Fig. 5, the reinforcements have the approximate aspect ratio of (a) six with 39.35 Å in length, (b) one with 7.38 Å and (c) 0.36 with 2.46 Å respectively. Accordingly, the carbon reinforcements used in this study are termed with respect to their aspect ratio, namely AR6, AR1 and AR0.36.

A bottom-up synthetic approach has been developed to overcome current issues with fabrication of CNTs[6] and to synthesize nanohoops[8,9] also known as cycloparaphenylene. This development may enable modeling the short carbon reinforcements shown in Fig. 5. The carbon atoms that form the structure of CNTs have sp^2 hybridised orbitals resulting in strong σ bonds as in CNTs. Although the development of the CNT reinforcements modelled in this study is still in progress, the estimated behavior of CNTs with the low aspect ratio in the epoxy was investigated with an implicit assumption that they will become available for mass-production in a short period of time.

Table 1 Comparison of molecular information for DGEBA model and commercial DGEBA

	EPON 825[28]	DGEBA in 7 gen. model
Average molecular weight/g mol^{-1}	355	354.6
Epoxide equivalent weight/g eq^{-1}	175–180	177.3
Average degree of polymerisation	$n = 1.05$	$n = 1.025$

Force field and functional form

The trajectories of particles during MD simulation in this study were calculated by a condensed-phase-optimized *ab initio* force field, COMPASS (condensed phase optimized molecular potentials for atomistic simulation studies)[29] throughout the whole MD simulation. COMPASS adopts the functional form to calculate the potential of the system from QMFF (quantum mechanical force field)[30] as shown in equation (1)

$$\begin{aligned} E_{\text{total}} = & \sum_{b}\left[K_{b2}(b-b_0)^2+K_{b3}(b-b_0)^3+K_{b4}(b-b_0)^4\right] \\ & +\sum_{\theta}\left[K_{\theta 2}(\theta-\theta_0)^2+K_{\theta 3}(\theta-\theta_0)^3+K_{\theta 4}(\theta-\theta_0)^4\right] \\ & +\sum_{\varphi}\left[K_{\varphi 1}(1-\cos\varphi)+K_{\varphi 2}(1-\cos 2\varphi)+K_{\varphi 3}(1-\cos 3\varphi)\right] \\ & +\sum_{\chi}K_{\chi}(\chi)^2+Cross\,Terms+\sum_{i,j}\frac{q_i q_j}{r_{ij}} \\ & +\sum_{i,j}\varepsilon_{ij}\left[2\left(\frac{r_{ij}^{*}}{r_{ij}}\right)^9-3\left(\frac{r_{ij}^{*}}{r_{ij}}\right)^6\right] \end{aligned} \quad (1)$$

where b is the bond length, θ is the bond angle, ϕ is the dihedral angle, χ is the out-of-plane angle and subscript 0 represents the reference value of each symbol. In the non-

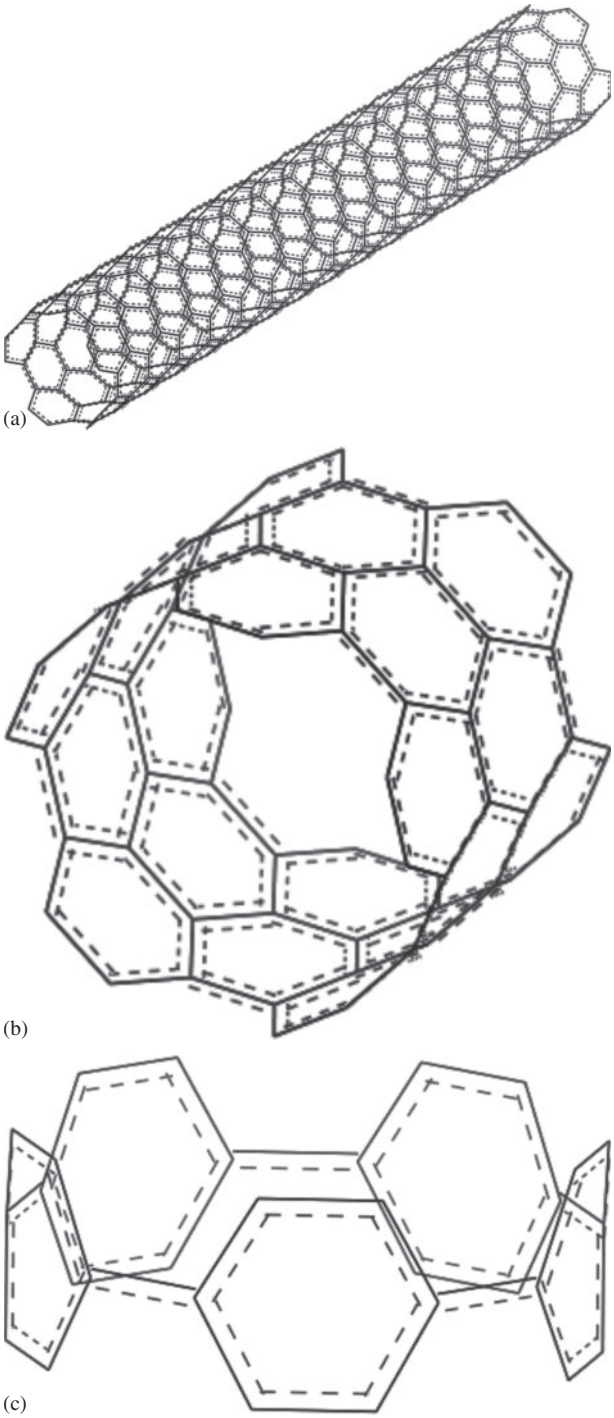

Figure 5 Atomistic sketch of carbon structures used in this study: *a* (5,5) single walled CNT with aspect ratio of 6 (AR6); *b* particle type (5,5) CNT with aspect ratio of 1 (AR1) and *c* CNT with aspect ratio of 0.36 (AR0.36)

bond energy terms, q, ε and r^* are the partial charge, depth of the well, and diameter of an atom respectively while van der Waals forces were calculated by the 9-6 Lennard-Jones function. The force-field parameterization in COMPASS is a hybrid process consisting of *ab initio* parameterization and empirical optimization.[29] Types of the atoms used in the model are shown in Fig. 2*b* and the definitions of each atom in the model are elaborated in Table 2 for reproduction of future investigators.

Packing in an amorphous cell and simulated annealing for equilibration

The seven generation cross-linked dendrimeric model described in the section on `Modeling constituents of epoxy and its crosslinking' underwent the geometry optimization process by energy minimization. Steepest descent was used for 10 000 iterations with the assumption that the initial configuration built in the dendrimer method was distant from the minimum energy surface. The structure was then further optimized by Quasi-Newton with a maximum of 40 000 iterations until a change in energy between consecutive iterations was less than 0.001 kcal mol^{-1}. To maintain the same weight fraction of 3 percent regardless of the reinforcement type, the carbon reinforcements with the different number depending on their molecular weight were packed with two of the optimized seven generation dendrimeric epoxy model in a three dimensional periodic boundary cell at the density of 0.4 g cm^{-3} to avoid discontinuous surface effects. This process was iterated six times for each arrangement to avoid dependency on the initial configuration and secure several local minima resembling the probable global optimum. Simulated annealing was carried out to densify the epoxy systems and to approximate the global potential energy state. The simulated annealing used in this study starts at the high temperature to prevent the system from being trapped in the neighborhood of local energy minima and to explore a larger configurational space until the temperature reduces gradually to room temperature.

A series of NVT (constant number of particles, volume and temperature) and NPT (constant number of particles, pressure and temperature) simulations for 0.5 ns was conducted with the integration time-step of 1 fs from 650 K with a decrement of 50 K until the system equilibrated at 298 K and atmospheric pressure. The time-step of 1 fs was chosen by monitoring conservation of potential energy in NVE (constant number of particles, volume and energy) ensemble and it was used throughout the study unless otherwise stated. The temperature and pressure of the molecular models were regulated by Andersen thermostat[31] and Berendsen barostat[32] to prevent undesirable changes in the shape of the simulation cell with a cut-off radius of 12.5 Å for the group-based summation. These temperature and pressure control methods were used throughout the whole MD simulation procedure. The volume occupied by the molecules of the constituents was calculated to get the fraction of free volume in the simulation cell with a probe radius of 1.4 Å for the solvent accessible surface area. The probe radius was defined by the van der Waals radii of the elements of interest, namely the nitrogen and oxygen atoms. A representative model with the epoxy reinforced by CNTs with AR0.36 and the free volume in the simulation cell is presented in Fig. 6. It should be noted that the free volume calculation does not involve the volume inside the CNT walls as the inner volume is not accessible by the bulky epoxy molecules. The molecular properties of the resulting structures are listed in Table 3. The properties shown in Table 3 resulted from the average of six frames for each configuration. A trend is observed from the free volume calculated for each material system that the bigger reinforcement

Table 2 Atom types used in this study

Material	General class	Atom	Type
Epoxy resin	Hydrogen types	h1	Nonpolar hydrogen
		h1o	Hydrogen bound to oxygen or fluorine
	Carbon types	c	Generic carbon
		c3a	Carbon, sp^2 hybridised aromatic
		c44	Carbon, sp^3 hybridised with 4 heavy atoms
		c4o	Carbon, sp^3 hybridised bonded to oxygen
	Nitrogen types	n3	Nitrogen, sp^3 hybridised in amines
	Oxygen types	o1 =	Oxygen, sp^2 hybridised in carbonyl
		o2e	Oxygen, sp^3 hybridised in ethers
		o2h	Oxygen, sp^3 hybridised in alcohol
	Sulphur types	s4 =	Sulphur, 4 bonds with 2 double bonds
Carbon structures	Carbon types	c	Generic carbon
		c3a	Carbon, sp^2 hybridised aromatic

results in the higher free volume in the cross-linked epoxy domain. These results agree with the experimental study[33] supporting the finding that the larger interfacial area of nano-contents leads to the higher free volume in the resin.

MD simulation

The simulation algorithms used in this study were scripted by Perl programming language, which in turn was interpreted by MaterialsScript Application Programming Interface in Materials Studio 6.0. The simulation methodology used in the study is divided into two categories, namely dynamic analysis for thermal properties and static analysis for mechanical properties. The dynamic analysis algorithm was developed earlier by the authors[11] for evaluation of thermal properties of material system. Each of the simulation-ready cells was equilibrated at 800 K by increasing the system temperature with an increment of 50 K for the sufficient time of 0.5 ns using an NPT ensemble under atmospheric pressure. The system temperature of the equilibrated structures was then dropped progressively by 10 K until the temperature reached 100 K while the variation in volume of the system under a temperature change was traced. The simulation period of 100 ps between the temperature changes was used and the last 20 ps was considered as a production period from which the trajectories were averaged for the required volumetric property.

A static approach was implemented for the mechanical property simulation with a strain-controlled algorithm. A limitation of the Berendsen barostat is that a change in a cell shape is infeasible so that stresses in each direction cannot be controlled separately. For this reason, the strain-controlled algorithm changed the individual length in each axis of the simulation cell. The global pressure tensor was then calculated and translated into the Cauchy stress tensor by Virial theorem[34] to extract responses of stress to the strain change in each direction. The new cell lengths in transverse directions were determined based on equation (2)

$$L_{y,z} = L_0(1 + \varepsilon_x)^{-\eta} \tag{2}$$

where L_0 is the initial length of the cubic cell, ε_x is the strain in the longitudinal direction and θ is the strain control factor. First, the strain was controlled with the strain control factor of (1. The simulation cell was stretched up to 5% strain for isotropic expansion to define the Poisson's ratio of the systems prior to the mechanical property simulation. Each simulation cell was strained at a constant rate of $2 \times 10^9\ s^{-1}$ and then relaxed for 10 ps after each strain variation. The stress responses over the last 2 ps of the relaxation process were averaged and Poisson's

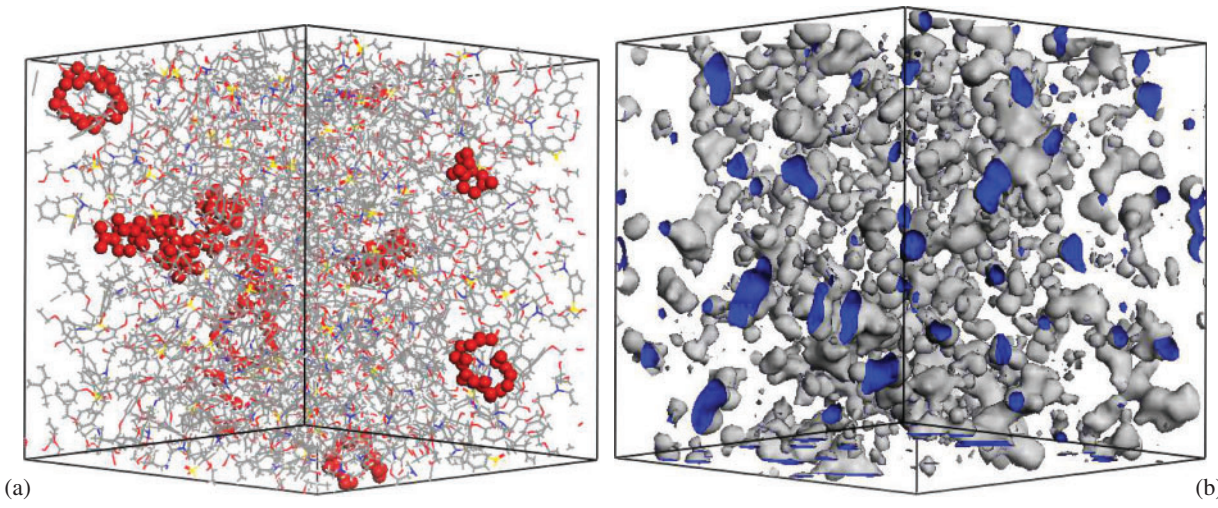

Figure 6 ***a*** **DGEBA/3,3'-DDS model with 3 wt-% of CNTs with AR0.36 in three-dimensional periodic boundary cell and** ***b*** **free volume of** ***a*** **with occupying molecules being hidden**

Table 3 Properties of simulation ready cells for each configuration after equilibration

	Neat epoxy	with CNT AR6	with CNT AR1	with CNT AR0.36
No. of reinforcement	0	1	6	11
No. of atoms	18866	19534	19554	19554
Density/g cm^{-3}	1.176 ± 0.003	1.202 ± 0.003	1.185 ± 0.001	1.180 ± 0.001
Cell length/Å	57.86	58.01	58.32	58.40
Free volume fraction	0.063 ± 0.007	0.081 ± 0.012	0.075 ± 0.008	0.067 ± 0.006

ratio for each material system was calculated based on the average stress in the longitudinal and transverse directions. The Poisson's ratio for each material system from the isotropic expansion simulation was taken for the strain control factor in equation (2) for the mechanical property simulation. The simulation-ready cells were again strained at the same rate up to 25% strain at 300 K while the trajectories of the MD simulation were stored over the production run at a sampling rate of 10 fs^{-1} in the NVT ensemble.

Evaluation of trajectories and discussion

The MD trajectories resulting from the simulated annealing were analyzed and their results are presented in this section. Each simulation set was repeated six times for each of six frames to maintain the statistical significance of the results. The initial velocity of particles at the given temperature in the atomistic models was defined by the Maxwell–Boltzmann distribution.

Glass transition temperature and coefficient of thermal expansion

The glass transition temperature T_g of each material system is identified in this section. T_g is one of the most important properties of amorphous materials since T_g differentiates the glassy phase from the rubbery phase that causes a loss of structural integrity of amorphous materials. The trajectories of the periodic simulation cells that underwent the thermal property simulation at the cooling rate of 0.1 K ps^{-1} were sampled every 10 simulation steps (i.e. every 10 fs) for the last 20% from the isothermal and isobaric simulation. The high sampling resolution was used to secure a great number of simulation data points because the molecular structures may fluctuate under changes in temperature even with the long period of equilibration. The variation in specific volume (the reciprocal of density) of each system under changes in temperature was calculated from the trajectory obtained in the

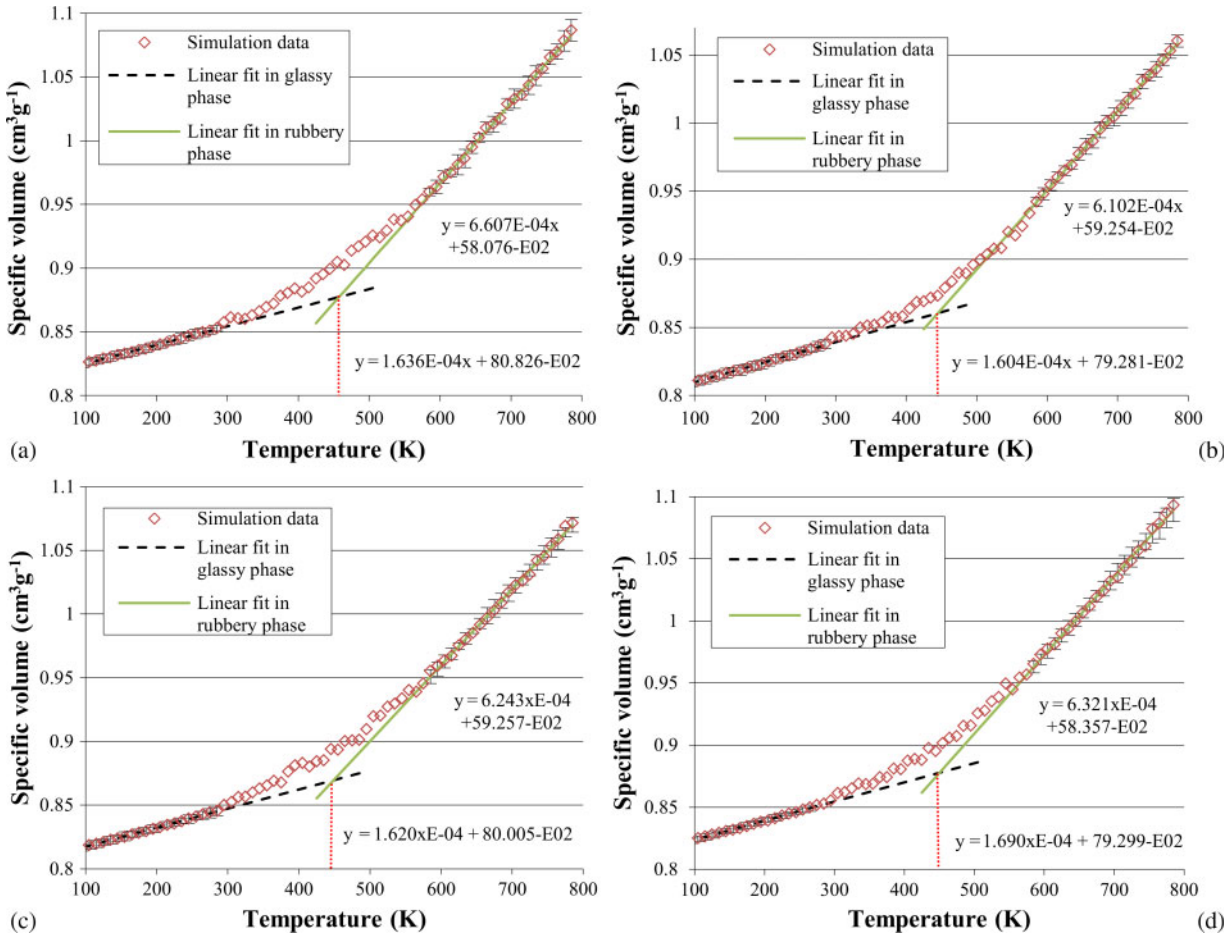

Figure 7 Specific volume as function of temperature for material systems *a* neat epoxy *b* with CNT AR6 *c* with CNT AR1 and *d* with CNT AR0.36

MD simulation. A linear regression analysis was conducted in the distinctive glassy (from 100 to 300 K) and liquid region (from 600 to 800 K) to get the representative linear graph in both the phases. T_g for each material system was determined from the intersection between the linear graphs as shown in Fig. 7.

The coefficient of thermal expansion (CTE) has been widely used as an indicator of thermal stability of materials.[35,36] The smaller CTE means that the material deforms less for a temperature change than those have a higher CTE. The volumetric CTE can be calculated from the same trajectories in the thermal property simulation under constant pressure by equation (3)

$$\alpha_V = \frac{1}{V_0}\left(\frac{\partial V}{\partial T}\right)_P \quad (3)$$

where V_0 is the initial system volume prior to the quenching process. The volumetric strain, $\Delta V/V_0$, can be obtained from the specific volume–temperature graphs in Fig. 6 as the mass of system was conserved during the simulation without a change in shape of the cell. Owing to the nature of the barostat used in this study, the simulation cell was expanded in an isotropic manner by which the coefficient of volumetric thermal expansion (the gradient in the glassy phase of the graphs from Fig. 6) can be converted to the linear CTE by $\alpha_L = \alpha_V/3$ as shown in Table 4. The results demonstrate that the CNT-type reinforcements have lowered T_g of the nanocomposites at elevated temperatures.

The T_gs of the epoxy-based nanocomposites were sensitively affected by the size of the CNT reinforcements. The T_gs decreased linearly with the increasing aspect ratio of the CNTs. Furthermore, the CNT additives with greater than 1 aspect ratio led to a small reduction in the CTE while the CTE for the nanocomposite reinforced by CNTs with AR0.36 was higher than that of the neat epoxy. The molecular network formed by CNT additives would restrain shrinkage of the epoxy molecules during the simulated annealing. However, it is relatively difficult to conclude whether the marginal changes in CTE are caused from the lower crosslinking density or the extremely low or even negative CTE of CNTs.[37] In combination with the free volume study shown earlier, the slightly higher CTE of the epoxy reinforced by CNTs with AR0.36 can be caused by the free volume from the evenly distributed small CNTs with AR0.36 allowing the extra space for the epoxy molecules to expand at the elevated temperatures.

Mechanical property

The trajectories that resulted from the constant stain controlled simulation were analyzed. Unlike continuum analysis, any of material systems at the nano-length scale cannot be isotropic in the discrete analysis. Therefore, the three-dimensional simulation cells were deformed with uniaxial tensile strain alternately along all three directions and results were averaged to avoid any anisotropic effects of the carbon reinforcement on final properties. As mentioned above, the deformation in the transverse direction was controlled by Poisson's ratio defined from the isotropic expansion simulation. The stress–strain relationship of each material is illustrated in Fig. 8. It is observed that the longer reinforcement provides the stiffer slope of the linear portion in the stress–strain curves while the neat epoxy provides the gentlest gradient. It can be interpreted that the CNT structures with the higher aspect ratio can impart more effective stiffening performance over the neat epoxy. Young's moduli of the materials were defined by a linear fit of the stress-strain curve within the strain range from 0 to 5 %. The resultant Young's moduli are shown in Table 4 together with yield strength and strain at 0.2% offset. As depicted in Fig. 8, the reinforcements with higher aspect ratio provide the better stiffening effect, evidenced by stiffer curves in the elastic region with higher stress. Several investigators[1,2,4,5] have reported that the stiffening effect of CNTs on a thermosetting polymer depends on the dispersal state of CNTs in the epoxy. Perfect dispersion is a property of the simulation but is harder to achieve experimentally. On the other hand, the CNT reinforcement accelerates the yield and the phenomenon becomes severer with the higher aspect ratio CNTs.

Evolution of potential energy under deformation

Evolution of major internal energy contributions during straining were calculated using equation (1) to understand further how the internal energy varies between the material systems under stretch. Interestingly, the contribution to changes in the potential energy by bond-length and bond-angle is not significant under deformation. The simulation results show that the large portion of deformation energy is accommodated by van der Waals and dihedral interactions. On the energy evolution during straining amorphous polymer, Capaldi *et al.*[38] has reported that the increase in stress of system is accompanied by a sharp increase in the dihedral angle transition rate and a pronounced change in dihedral angle transition rate immediately after yield. While the direct comparison of changes in energy between different systems might be meaningless, correlation of energy decompositions can be found with changes in the response of stress (Fig. 8) to strain in the system. The dihedral energy steadily increases within the elastic region and it might determine the plastic behavior of the materials in conjunction with van der

Table 4 Simulation results from thermal and mechanical property algorithm

	Neat epoxy	With CNTs AR6	With CNT AR1	With CNT AR0.36
CTE in glassy phase/$10^{-6}K^{-1}$	54.5 ± 1.1	53.4 ± 0.7	54.0 ± 1.4	56.4 ± 1.2
CTE in rubbery phase/$10^{-6}K^{-1}$	220.24 ± 3.4	203.40 ± 5.3	208.10 ± 3.0	210.69 ± 4.7
T_g/°C	184.5 ± 3.2	172.2 ± 6.2	175.7 ± 2.4	179.1 ± 3.5
Poisson's ratio	0.38	0.33	0.34	0.37
Young's modulus/Gpa	2.5 ± 0.0	3.0 ± 0.0	2.7 ± 0.0	2.7 ± 0.1
Yield strength/Mpa	140.6 ± 5.5	159.4 ± 4.5	141.1 ± .6.5	150.4 ± 7.2
Yield strain	0.064 ± 0.002	0.052 ± 0.006	0.056 ± 0.004	0.060 ± 0.008

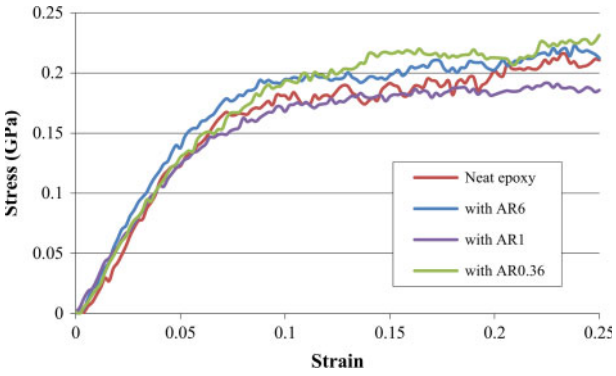

Figure 8 Stress–strain response of neat and CNT modified epoxy

Waals energy. When the combination of van der Waals and dihedral energy increases the stress-strain curve shows strain hardening, and vice versa. Similar results have been reported in the literature[39,40] that attributes the results to conformational changes from the gauche state to the lower energy level trans state. The energy decomposition in Fig. 9 demonstrates that the lengthy CNTs delayed both the van der Waals and dihedral energy leveling out.

Degree of crosslinking by analyzing local structures

Bulk density of the final structure resulting from the MD simulation has often been used to measure the degree of crosslinking.[10,11,15,16] A direct comparison of bulk density is not applicable to the nanocomposites reinforced by additives that have dramatically different density to that of resins. Therefore, this study focuses on the probability of crosslinks in the three-dimensional epoxy domain to investigate the effect of the reinforcing CNT structures on the crosslinking density of the epoxy resin. There are a number of approaches to define the degree of crosslinking, such as swelling[41] and the average molecular weight of crosslinks[42,43] based on the rubber elasticity theory. On the other hand, some of previous investigations[15,16,44] have dealt with the progression of the local structure during the curing process to compare the degree of crosslinking for each system by the pair distribution function (PDF). The PDF of the nitrogen atom (n3 in Table 2) in the amine group and the oxygen atom (o2h in Table 2) in the hydroxyl group, generated from the formation of a covalent bond between DGEBA and 3,3'-DDS, was used in this study. The PDF provides information on the probability for existence of a particle as a function of distance from a reference particle with its center located in a spherical shell of an infinitesimal thickness at a distance (r) as defined in equation (4)[45]

$$g_{NO}(r) = \frac{1}{x_N x_O \rho}\left\langle \frac{1}{N}\sum_{i=1}^{N_N}\sum_{j=1}^{N_O}\delta(r - r_i + r_j)\right\rangle \quad (4)$$

where x_N and x_O are the mole fraction of nitrogen and oxygen designated earlier respectively, N_N and N_O are the

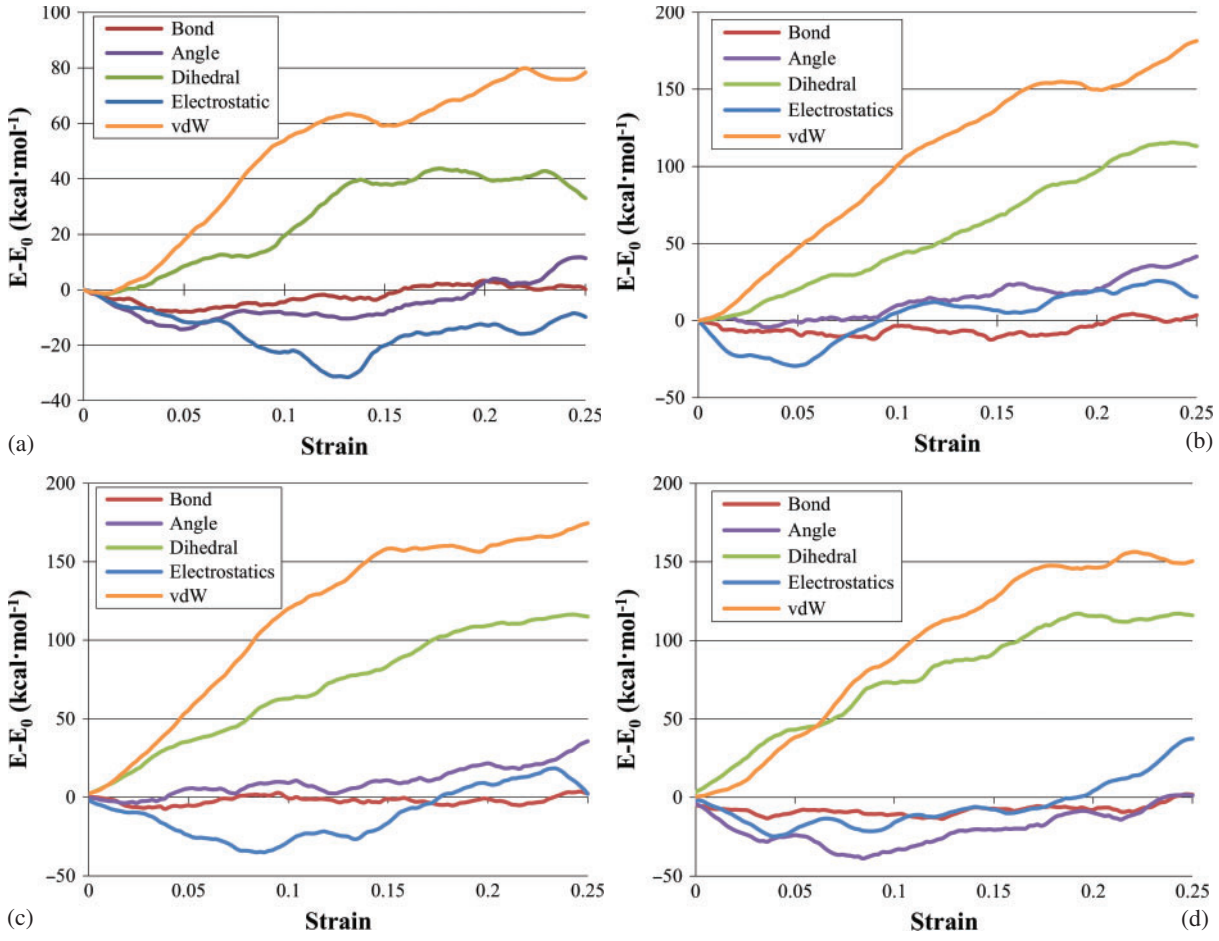

Figure 9 Decomposition of potential energy under deformation *a* neat epoxy *b* with CNT AR6 *c* with CNT AR1 and *d* CNT AR0.36

number of the same nitrogen and oxygen respectively, and ρ is the overall density of the molecular model. The angle brackets imply the configurational average of the system and *N* is the total number of the nitrogen and oxygen atoms. The summation of intra- and inter-molecular PDF of N-O correlation is depicted in Fig. 10. As in the literature[15] using the same epoxy system, the first three peaks are observed at 3, 3.8 and 4.3 Å as a result of covalent bond creation. Owing to the same conversion rate throughout the whole simulation procedure, the peaks are positioned at these radii. However, the probability of finding N or O atoms within certain radii from the reference atom distinctively increases with the same order in the T_gs in Table 4 until the average number of atoms becomes proportional to the shell volume. These results can be interpreted that the bulkier reinforcement in the cross-linked epoxy causes a less dense local structure due to its physical hindrance in the three-dimensional domain potentially reducing the degree of crosslinking of the thermosetting resin.

Conclusions

This paper elucidated a detailed methodology of modeling the atomistic structures of thermosetting epoxy and its crosslinking process with the CNT reinforcements with various aspect ratios. The dendrimeric approach adopted in this investigation successfully mimicked the polymerization process of DGEBA crosslinked with 3,3'-DDS. Molecular dynamics was implemented to estimate the thermo-mechanical properties of the epoxy resin reinforced by the diverse CNTs at the constant weight fraction of 3%. The study on the configurational information of the average molecular trajectory from the simulated annealing for each nanocomposite showed that the higher aspect ratio reinforcements led to higher free volume in the local epoxy molecular domain.

The MD simulation provided the notable influence of the CNTs with AR6 increasing the elastic properties of the epoxy resin with compromising thermal properties. In contrast, the influence of CNTs with the lower aspect ratio was less pronounced. It is observed that inclusion of the CNT additives in the epoxy resin results in the lower glass temperature and CTE besides the epoxy reinforced by CNTs with AR0.36. In addition, the CNT reinforcements stiffen the epoxy matrix and increase the strength, whereas reducing the strain at yield. The focus of the study was then directed to the investigation of the causes for the MD simulation results. The averaged free volume from a series of equilibrated trajectories presented the indirect relationship between the size of the CNT-additives and the crosslinking density since the increase in free volume is proportional to the aspect ratio of the additives. The pair distribution function study for the amine and epoxide group demonstrated the similar results that the pristine epoxy resin provides the densest molecular configuration followed by the material system with the smallest reinforcements. This allows us to induce that the steric hindrance of the bulky CNT structures to densification of the local epoxy molecular domain causes the lower crosslinking density, allowing more free volume. This may result in more space under the same annealing and equilibration process. The additional space occurred from packing CNTs with the epoxy may increase the mobility of polymer chains for an easier long range segmental motion facilitating earlier transition at elevated temperatures. However, the existence of CNT additives in the epoxy directly provides the higher stiffness and strength under deformation. The evolution of energy decomposition as a function of strain indicates that torsional movement of the epoxy molecules was impeded by the physical obstruction of the CNT additives which leads to delaying the energy state moving to the lower state. The results from this investigation can be implemented to impart the general idea of the influence of CNTs that are currently used or other nanoscale reinforcements on the crosslinking behavior of the epoxy resin.

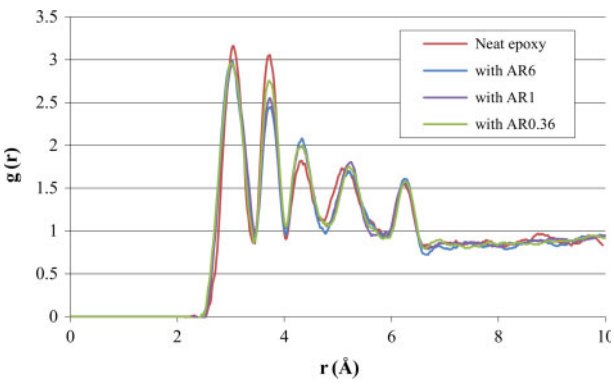

Figure 10 Pair distribution function for N in amine group and O in hydroxyl resulting from crosslinking process

Conflicts of interest

The authors have no conflicts of interest to declare.

Acknowledgements

The authors wish to thank Stephen Christensen and Andrea Browining from the Boeing Company for their guidance on the thermosetting resin modeling approach and helpful discussions.

References

1. A. Jiménez-Suárez, M. Campo, I. Gaztelumendi, N. Markaide, M. Sánchez and A. Ureña: *Compos. Part B-Eng.*, 2013, **48**, 88–94.
2. J. A. Kim, D. G. Seong, T. J. Kang and J. R. Youn: *Carbon*, 2006, **44**, (10), 1898–1905.
3. F. H. Gojny and K. Schulte: *Compos. Sci. Technol.*, 2004, **64**, (15), 2303–2308.
4. Y. S. Song and J. R. Youn: *Carbon*, 2005, **43**, (7), 1378–1385.
5. H. Miyagawa and L. T. Drzal: *Polymer*, 2004, **45**, (15), 5163–5170.
6. M. Kumar and Y. Ando: *J. Nanosci. Nanotechnol.*, 2010, **10**, (6), 3739–3758.
7. R. Rafiee and R. Pourazizi: *Mater. Res.*, 2014, **17**, 758–766.
8. S. Hitosugi, W. Nakanishi, T. Yamasaki and H. Isobe: *Nature Commun.*, 2011, **2**, 492.
9. T. J. Sisto and R. Jasti: *Synlett*, 2012, (04), 483–489.
10. C. Wu and W. Xu: *Polymer*, 2006, **47**, (16), 6004–6009.
11. J. -H. Sul, B. G. Prusty and D. W. Kelly: *Compos. A-Appl. S.*, 2014, **65**, 64–72.
12. S. Christensen: `Atomistically explicit molecular dynamics simulation of thermosetting polymers', Proc. 39th ISTC SAMPE Conf., Cincinnati, OH, USA, October–November 2007, SAMPE. 2007. ISBN: 978-1-934551-01-1.
13. N. Nouri and S. Ziaei-Rad: *Macromolecules*, 2011, **44**, (13), 5481–5489.
14. C. Li and A. Strachan: *Polymer*, 2010, **51**, (25), 6058–6070.
15. A. Shokuhfar and B. Arab: *J. Mol. Model.*, 2013, **19**, (9), 3719–3731.
16. S. Yang and J. Qu: *Polymer*, 2012, **53**, (21), 4806–4817.
17. A. Haque and A. Ramasetty: *Compos. Struct.*, 2005, **71**, (1), 68–77.
18. K. K. H. Wong, M. Zinke-Allmang, J. L. Hutter, S. Hrapovic, J. H. T. Luong and W. Wan: *Carbon*, 2009, **47**, (11), 2571–2578.
19. R. Zhu, E. Pan and A. K. Roy: *Mater. Sci. Eng.*, 2007, **447A**, (1–2), 51–57.

20. B. Coto, I. Antia, J. Barriga, M. Blanco and J. -R. Sarasua: *Comput. Mater. Sci.*, 2013, **79**, 99–104.
21. N. Pal, D. Srivastava and J. S. P. Rai: *J. Appl. Polym. Sci.*, 2010, **117**, (4), 2406–2412.
22. G. Liang, P. Ren, Z. Zhang and T. Lu: *J. Appl. Polym. Sci.*, 2006, **101**, (3), 1744–1750.
23. C. D. Caroselli, M. Pramanik, B. C. Achord and J. W. Rawlins: *High Perform Polym.*, 2012, 1–12.
24. Accelrys Inc., Materials Studio 6.0, San Diego: Accelrys Inc., 2011.
25. A. K. Rappe and W. A. Goddard III: *J. Phys. Chem.*, 1991, **95**, (8), 3358–3363.
26. A. R. Leach: `Molecular modelling: principles and applications'; 1996, Harlow, Addison Wesley Longman.
27. A. R. Browning: `Utilization of molecular simulations in aerospace materials: simulation of thermoset resin/graphite interactions', Proc. 2009 AIChE Annual Meeting, 09AIChE, November 2009, Nashville, TN, USA, 2009, American Institute of Chemical Engineers.
28. MOMENTIVE, Available at: http://www.momentive.com/Products/TechnicalDataSheet.aspx?id=;3936, Technical Data Sheet, 2005 [accessed 30 June 2014].
29. H. Sun: *J. Phys. Chem. B*, 1998, **102B**, (38), 7338–7364.
30. J. R. Maple, M. J. Hwang, T. P. Stockfisch, U. Dinur, M. Waldman, C. S. Ewig and A. T. Hagler: *J. Comput. Chem.*, 1994, **15**, (2), 162–182.
31. H. C. Andersen: *J. Chem. Phys.*, 1980, **72**, (4), 2384–2393.
32. H. J. C. Berendsen, J. P. M. Postma, W. F. van Gunsteren, A. DiNola and J. R. Haak: *J. Chem. Phys.*, 1984, **81**, (8), 3684–3690.
33. D. H. Yu, B. Wang, Y. Feng and Z. P. Fang: *J. Appl. Polym. Sci.*, 2006, **102**, (2), 1509–1515.
34. M. Zhou: *Proc. Mathemat. Phys. Eng. Sci.*, 2003, **459**, (2037), 2347–2392.
35. K. C. Yung, B. L. Zhu, T. M. Yue and C. S. Xie: *J. Appl. Polym. Sci.*, 2010, **116**, (1), 225–236.
36. M. Cho, J. Jang and J. Suhr: *J. Nanosci. Nanotechnol.*, 2011, **11**, (2), 1098–1102.
37. S. Wang, Z. Liang, P. Gonnet, Y. -H. Liao, B. Wang and C. Zhang: *Adv. Funct. Mater.*, 2007, **17**, (1), 87–92.
38. F. M. Capaldi, M. C. Boyce and G. C. Rutledge: *Phys. Rev. Lett.*, 2002, **89**, (17), 175505.
39. D. Hossain, M. A. Tschopp, D. K. Ward, J. L. Bouvard, P. Wang and M. F. Horstemeyer: *Polymer*, 2010, **51**, (25), 6071–6083.
40. T. Mulder, V. A. Harmandaris, A. V. Lyulin, N. F. A. van der Vegt, B. Vorselaars and M. A. J. Michels: *Macromol. Theor. Simul.*, 2008, **17**, (6), 290–300.
41. ASTM-International: `Standard test methods for determination of gel content and swell ratio of crosslinked ethylene plastics', ASTM Standard D2765, West Conshohocken, PA, USA; 2011.
42. B. U. Kang, J. Y. Jho, J. Kim, S. -S. Lee, M. Park, S. Lim and C. R. Choe: *J. Appl. Polym. Sci.*, 2001, **79**, (1), 38–48.
43. J. P. Bell: *J. Appl. Polym. Sci.*, 1970, **14**, (7), 1901.
44. J. S. Bermejo and C. M. Ugarte: *Macromol. Theor. Simul.*, 2009, **18**, (6), 317–327.
45. J. -P. Hansen and I. R. McDonald: 'Chapter 4 – distribution function theories, in Theory of simple liquids (fourth edition)', (ed. J. -P. Hansen, et al.), fourth edition, 105–147; 2013, Oxford, Academic Press.